Postprint of: Winiarz P., Mielewczyk-Gryń A., Lilova K., Wachowski S., Subramani T., Abramchuk M., Dzik E., Navrotsky A., Gazda M., **Conductivity, Structure, and Thermodynamics of $Y_2Ti_2O_7$-Y_3NbO_7 solid solutions,** ***Dalton Trans.***, vol. 49 (2020) pp. 10839-10850, **https://doi.org/10.1039/D0DT02156C**

Conductivity, Structure, and Thermodynamics of $Y_2Ti_2O_7$-Y_3NbO_7 solid solutions

Piotr Winiarz[1*], Aleksandra Mielewczyk-Gryń[1], Kristina Lilova[2], Sebastian Wachowski[1], Tamilarasan Subramani[2], Mykola Abramchuk[2], Ewa Dzik[1], Alexandra Navrotsky[2], Maria Gazda[1]

[1] Gdańsk University of Technology, Faculty of Applied Physics and Mathematics, Narutowicza 11/12, 80-233 Gdańsk, Poland
[2] School of Molecular Sciences and Center for Materials of the Universe, Arizona State University, Tempe AZ 85287 USA

[*]Corresponding author. E-mail: piotr.winiarz1@pg.edu.pl

Abstract

The defect-fluorite yttrium niobate Y_3NbO_7 and pyrochlore yttrium titanate $Y_2Ti_2O_7$ solid solutions have been synthesized via solid state synthesis route. The resulting stoichiometry of the oxides are $Y_{2+x}Ti_{2-2x}Nb_xO_7$, where x = 0 to x = 1. All of the samples were single-phase, however for these with predominant fluorite phase, a small amount of additional pyrochlore phase were detected. The volume of the solid solutions unit cells is linearly increasing with increasing yttrium niobate content. The water uptake is increasing with (x), and the protonic defects concentration reaches almost 4.5 x 10^{-3} mol/mol at 300°C. The calculated enthalpy of formation from oxides suggest strong stability for all of the compositions, with values of enthalpy ranging from -84.6 to -114.3 kJ/mol. The total conductivity does not have a visible dependence on Y_3NbO_7 content. For each compound, the total conductivity is higher in wet air. Interestingly, for samples where $x < 0.5$, ratio of conductivity in hydrogen to air is increasing with increasing temperature, while for $x > 0.5$, the trend is opposite.

Introduction

Solid solutions of oxides form when cations of one oxide occupy sites of the host oxide lattice, leading to occupancy by two or more species with potentially different states of short and long range order. For decades, the formation of solid solutions between various oxides has attracted much attention since this procedure enables tailoring structural and functional properties of materials. For example, in solid solutions of lead zirconate and titanate piezoelectric properties were optimized [1], in Ce-Zr-O system - catalytic properties [2], $Sr(Ti,Fe)O_{3-x}$ - optical [3] and electrical properties, while $Ba(Zr,Ce,Y)O_{3-x}$ have been studied to elaborate a proton-conducting electrolyte for applications in various electrochemical devices [4–6]. In this work, structure, energetics of formation, water uptake and electrical properties of the $(Y_3NbO_7)_x(Y_2Ti_2O_7)_{1-x}$ yttrium niobate - yttrium titanate solid solutions are presented. In the further text the equivalent $Y_{2+x}Ti_{2-2x}Nb_xO_7$ formula of the oxide will be used, where *x* signifies the mole fraction of yttrium niobate.

In oxides, similar to alloys in which Hume-Rothery rules describe the ability of elements to form a solid solution [7], the solubility limits depend mainly on the size, as commonly described by ionic radii, of the cations and preferred crystal structures of the oxides. In $Y_{2+x}Ti_{2-2x}Nb_xO_7$ cations that are expected to substitute for each other in the solid solution are niobium and titanium. Both Nb^{5+} in Y_3NbO_7 and Ti^{4+} in $Y_2Ti_2O_7$ occupy the sites with eightfold coordination and have the same ionic radii (0.74 Å) [8]. A comparison of crystal structures of the end members of the solid solution is less straightforward, however, both are, at least at the long range scale, high symmetry FCC structures. Yttrium niobate, Y_3NbO_7, crystallizes in the cubic defect fluorite structure – $(Fm\bar{3}m)$[9], whereas $Y_2Ti_2O_7$, in the cubic pyrochlore structure $(Fd\bar{3}m)$, so that they differ only in a symmetry plane. Unit cells of both oxides are presented in Fig. 1. The unit cell parameters of Y_3NbO_7 and $Y_2Ti_2O_7$ are 5.2495(1) Å and 10.095(1) Å, respectively [10, 11]. Since the pyrochlore unit cell contains eight whereas fluorite contains four molecules per unit cell, to compare unit cell parameters, that for the fluorite should be multiplied by 2. Therefore, the structural properties of Y_3NbO_7 and $Y_2Ti_2O_7$ suggest that forming a solid solution of these two oxides should be possible. Moreover, due to the cation ordering, pyrochlore may be regarded as 2 x 2 x 2 superstructure of the defect fluorite [12] with chemical formula $Y_{0.5}Ti_{0.5}O_{2-0.25}$.

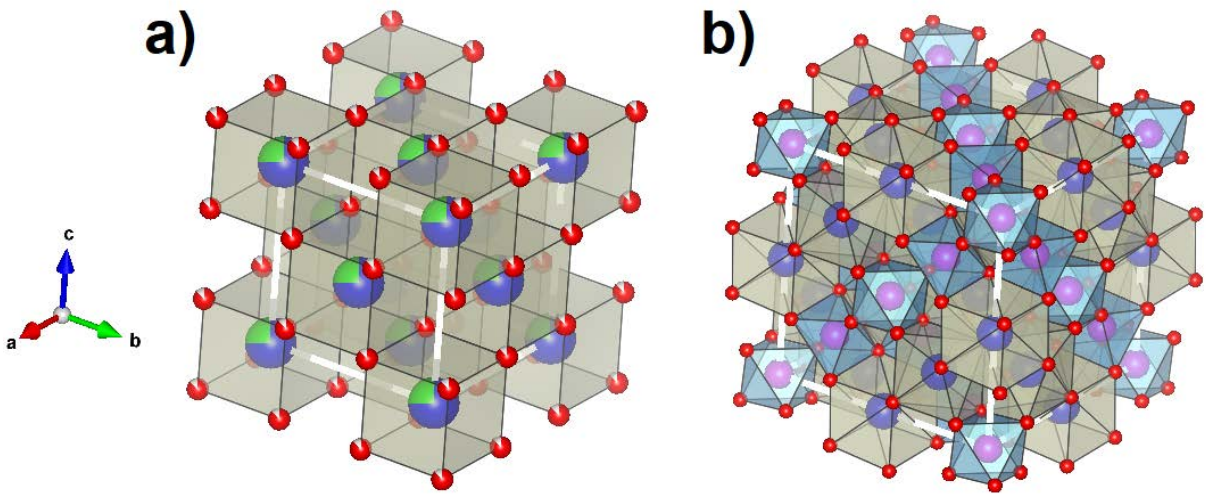

Figure 1 a) Y_3NbO_7 defect fluorite structure ($Fm\bar{3}m$). b) $Y_2Ti_2O_7$ pyrochlore structure ($Fd\bar{3}m$). Colors: blue – yttrium, green – niobium, red – oxygen, white – oxygen vacancies, purple – titanium. Unit cell edges are marked with thick white lines. Pictures prepared by Vesta Software[13].

Electrical properties of the $Y_{2+x}Ti_{2-2x}Nb_xO_7$ yttrium niobate and yttrium titanate solid solutions are expected to depend on the mole fraction (x) and electrical properties of the constituent oxides. Both Y_3NbO_7 and $Y_2Ti_2O_7$ are considered as oxygen ion and/or mixed ionic-electronic conductors. Yttrium niobate is recognized as an oxygen ion conductor in a wide oxygen partial pressures range[9], whereas in $Y_2Ti_2O_7$ at low pO_2 electronic conductivity surpasses ionic[14]. In both oxides, oxygen ion conduction occurs through oxygen vacancies, so that comparison of oxygen vacancy properties is relevant for conduction phenomena in the solid solution materials. In Y_3NbO_7, forming a defect fluorite structure, structural oxygen vacancies are present, which occupy different oxygen positions. Figure 1 schematically indicates that the vacancies are distributed randomly between the oxygen sites, however, Marrocchelli et al. [15] suggested they are likely to be close to yttrium 3+ rather than to niobium 5+ because the lower charge difference would be beneficial from the lattice energetics point of view. They found that in Y_3NbO_7 the Y-O bonds are weaker than the Nb-O so that oxygen vacancy formation requires lower energy in the neighborhood of yttrium. They also showed that the oxygen ions located in tetrahedral sites with all the vertices occupied by Y^{3+} cations are immobile [15]. In the $RE_2O_3 – CeO_2$ defect fluorites, oxygen vacancies tend to become ordered depending on the cation radii in the nearest neighborhood [16]. Holliday et al. have shown that in the defect fluorite

curium doped $La_2Zr_2O_7$, the presence of randomly distributed oxygen vacancies [17] leads to many possibilities of forming closely related cation sites.

To enhance the ionic conductivity of yttrium niobate, substitutions that can increase the concentration of oxygen vacancies may be applied. In our previous work, we showed that $Y_3Nb_{1-x}Ti_xO_{7-\delta}$ for x = 0 to x = 0.15 exhibits protonic conductivity[10]. Yttrium titanate also contains structural oxygen vacancies, however, in contrast to Y_3NbO_7 they occupy only one type of site, i.e. 8a (1/8, 1/8, 1/8). Moreover, as found by Xiao et al. with *ab initio* methods, these sites can also be occupied by cations [18]. The total conductivity of $Y_2Ti_2O_7$ in humidified air is higher than in dry air, indicating protonic conductivity, which was shown in a Ph.D. thesis [19]. The protonic conductivity is around 50 % of the total conductivity between 400 and 500 °C, and decreases with increasing temperature, to 1 % at 800 °C.

The aim of this work is the in-depth analysis of the influence of formation energetics on oxygen ion and proton conductivity to understand the relations between the complex solid solution structure, thermodynamics, and their electrical properties. This work is partially based on the thermodynamics of the Ce_nO_{2n-2m} defect fluorites (where n and m are integers, n > m) [20] and $RE_2Zr_2O_7$ pyrochlores – defect fluorites (RE = Sm, Eu, Gd) [21].

Experimental Methods

The samples of $Y_{2+x}Ti_{2-2x}Nb_xO_7$ for x = 1; 0.9; 0.8; 0.7; 0.6; 0.5; 0.4; 0.3; 0.2; 0.1 and 0, were prepared through a solid-state synthesis route. The following precursors of metal oxides were used and mixed in an agate mortar: Y_2O_3 (Alfa Aesar, 99.99 %); Nb_2O_5 (Alfa Aesar, 99.9985 %), and TiO_2 (VWR, 99 %). The resultant powders were uniaxially pressed into pellets, which were calcined in three steps: at 1350 °C for 8 h, then 1400° C for 12 h and the final sintering was performed at 1500 °C for 14 h. Between each annealing step, pellets were ground in an agate mortar and re-pelletized.

X-ray diffraction (XRD) was performed on a Phillips X'Pert PRO diffractometer with Cu Kα radiation (λ = 1.541 Å). The Rietveld refinement was carried out in HighScore Plus software. A pseudo-Voigt profile function was used to fit the data. As an initial point of the analysis, unit cell parameters of the fluorite and pyrochlore structure were used respectively

(space group no. 225, and 227) [22, 23]. Thermogravimetric analysis (TGA) was performed on sample powders using a Netzsch Jupiter® 449 F1. In each case, the mass of the specimen was approximately 2 g. Powders were heated to 1000 °C and held at this temperature for 0.5 h under dry synthetic air (N_2/O_2 80/20) to remove residual water and possible surface carbon dioxide. The samples after drying were cooled to 300 °C in dry gas. After 2 hours of stabilization, dry gas was switched to the humidified gas (pH_2O = 0.023 atm.), then after an additional 2 h, the gas was switched back to the dry gas. High-temperature oxide melt solution calorimetry was performed using a Tian Calvet twin-type calorimeter AlexSYS (Setaram, France) at 800 °C. The samples were pressed into pellets and dropped into a platinum crucible containing molten sodium molybdate $3Na_2O{\cdot}4MoO_3$ solvent. Oxygen gas was flushed over the solvent at 90 ml/min and bubbled through it at 5 ml/min. The calorimeter was calibrated against the heat content of 5 mg pellets of Al_2O_3. This methodology is well established and has been described previously [24]. Electrochemical impedance spectroscopy data (EIS) were obtained with a Gamry Reference 3000 Potentiostat/Galvanostat in the frequency range 1Hz – 1MHz and temperature range 400 – 800 °C with 50 °C steps. Measurements were taken in dry/wet air and dry/wet hydrogen. Nyquist plots were fitted using ZView software (Scribner Associates) with an R/(RQ)/(RQ) equivalent circuit model.

Results and Discussion

Figure 2a depicts the X-ray diffractograms of yttrium niobate - yttrium titanate solid solutions.

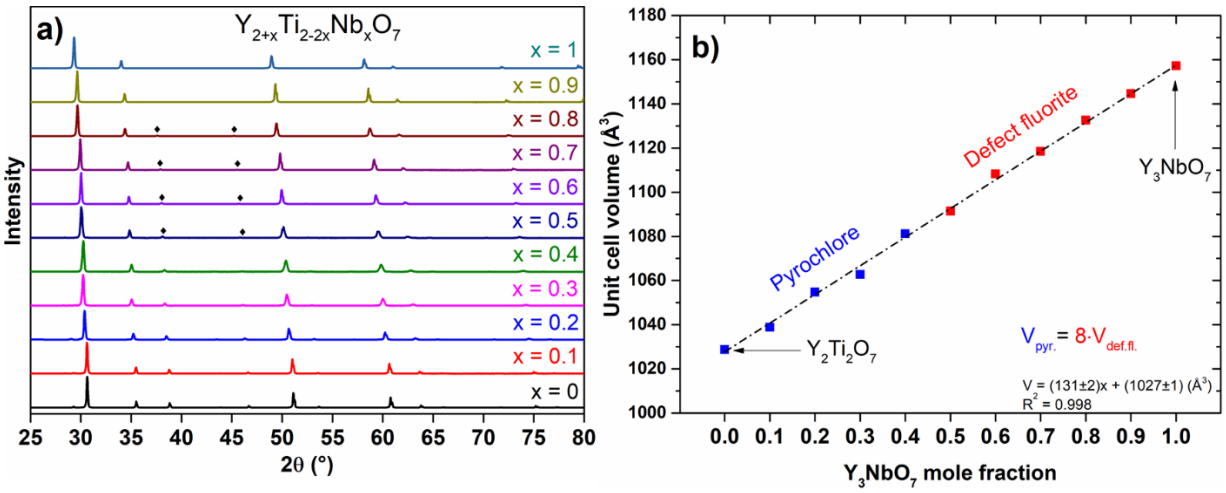

Figure 2 a) X-ray diffractograms of synthesized $Y_{2+x}Ti_{2-2x}Nb_xO_7$ solid solutions. Black diamonds mark the reflections around 38° and 47° which correspond to additional pyrochlore ordering, b) normalized volume of the unit cell of $Y_{2+x}Ti_{2-2x}Nb_xO_7$.

The results show that the investigated system forms a single-phase solid solution in the whole range of (x), although they crystalize in different systems: defect fluorite and pyrochlore. The structural analysis shows that the solid solution samples for x between 0 to 0.4, exhibit pyrochlore structure, while for 0.5 to 1 show defect fluorite structure. However, for the $Y_{2.5}Ti_{1.0}Nb_{0.5}O_7$, $Y_{2.6}Ti_{0.8}Nb_{0.6}O_7$, $Y_{2.7}Ti_{0.6}Nb_{0.7}O_7$, and $Y_{2.8}Ti_{0.4}Nb_{0.8}O_7$ samples, additional very weak reflections around 38 ° and 47 ° are visible. The reflections may be attributed to the pyrochlore structure, however, they suggest additional ordering in the cation sublattice, not the presence of the pyrochlore secondary phase. Such a phenomenon has been previously reported for RE_3NbO_7 (RE = Y, Er, Yb, Lu) rare earth niobates by López-Conesa [9], who suggested the presence of domains with short-range pyrochlore ordering in the structure. Also in the $Gd_2(Zr_{1.5}Ce_{0.5})O_7$ defect-fluorite high energy electron microscopy investigations showed the presence of small pyrochlore domains [25]. Similarly, for zirconia, hafnia, ceria and similar fluorite-type oxides, it has been shown that pyrochlore microdomains are forming locally[26].

Generally, oxides forming the defect fluorite and pyrochlore structures present a variety of interesting structural properties. For example, they often form solid solutions. Liu et al., have shown that, depending on the zirconium content in $Y_2(Zr_yTi_{1-y})_2O_7$ [27], the compounds crystallize in defect fluorite or pyrochlore structure but appear to form a solid solution in the whole range. In the case of $(1-x)\cdot ZrO_2 - x\cdot GdO_{1.5}$, the solid solution forms for x between 0.33 and 0.6 [28]. On the other hand, in the case of single-phase solid solutions of $Gd_2(Zr_{2-x}Ce_x)O_7$ system, the structure changes from pyrochlore ($x < 0.25$) to defect-fluorite ($x = 0.5, 0.75$) with increasing cerium content [25].

Figure 2b presents the normalized unit cell volume of the synthesized solid-solutions. To compare the volumes, since the pyrochlore unit cell contains more molecules per unit cell than fluorite, the volume of the latter has been multiplied by 8. One can see that despite the change of the structure symmetry, the dependence of the unit cell volume vs x is continuous and linear in the whole range, with no indication of any discontinuity at the symmetry change. This observation supports treating the whole system as a single solid solution. This continuity can be explained by the fact that in both of the structures the BO_6 octahedra have a major influence on the size of the unit cell [29] and both of the B-site cations, namely Ti^{4+} and Nb^{5+}, have the same radii.

The unit cell volume depends linearly on x, the volumetric chemical expansion coefficient of Y_3NbO_7 dissolution in $Y_2Ti_2O_7$, can be calculated by fitting the formula into the unit cell volume dataset (1) [30]:

$$\beta_{dis.} = \frac{1}{x} \cdot \frac{V - V_0}{V_0} \quad (1)$$

Where x is Y_3NbO_7 mole fraction, V is the normalized unit cell volume for x, and V_0 is the volume determined for $x = 0$. $\beta_{dis.}$ is a refinable parameter representing the slope of relative volume increase plotted as a function of x and it is the chemical expansion coefficient of dissolution. The volume increases linearly for the whole range, therefore the chemical expansion coefficient is constant in the whole range and equals $\beta_{dis.} = 0.127 \pm 0.004$. In comparison, the chemical expansion coefficient for fluorite $CeO_{2-\delta}$ is around 0.1 [31], however the coefficient was estimated from expansion changes as a function of the stoichiometry of oxygen ions δ.

The water uptake has been studied by thermogravimetry, in which the mass gain upon switching from dry to wet air at 300 °C has been determined. For the whole system, protonic defects form when water vapor reacts with the material, according to equation (2).

$$H_2O_{(g)} + V_O^{\bullet\bullet} + O_O^X \rightarrow 2OH_O^{\bullet} \quad (2)$$

On this basis, the proton concentration $[OH_O^{\bullet}]$ has been calculated using equation (3):

$$[OH_O^{\bullet}] = \frac{2 \cdot M \cdot \Delta m}{M_{H2O} \cdot m_0} \quad (3)$$

where M is the molar mass of the compound, Δm is the difference between the mass of the hydrated sample and mass before the gas switch, M_{H2O} is the molar mass of water and m_0 is the mass of the sample. The water uptake and resulting proton concentration are presented in Figure 3. The water uptake in $Y_{2+x}Ti_{2-2x}Nb_xO_7$ compounds increases with increasing *(x)*. The protonic defect concentration in Y_3NbO_7 is almost $4.5 \cdot 10^{-3}$ mol/mol, whereas for $Y_2Ti_2O_7$ it is around 10^{-3} mol/mol. Nevertheless, the water uptake for the solid solution is quite low and smaller than that observed for barium zirconate - barium cerate solid solutions[32]. In comparison, the water uptake effect in fluorite-pyrochlore $(La_{1-y}Ca_y)_2(Ce_{1-x}Zr_x)_2O_{7-\delta}$ compounds is higher for more disordered systems, contrary to our samples [33]. On the other hand, the water uptake is of the same order of magnitude as for the lanthanum orthoniobate system which exhibits considerable protonic conductivity in a wide range of temperature and oxygen partial pressures [34, 35]. For the $La_2Ce_2O_7$ pyrochlore, the protonic defects concentration at 300 °C is around $3 \cdot 10^{-2}$ mol/mol [36]. In rare-earth niobates RE_3NbO_7 (RE = Y, Yb, Lu, Gd, and La) the water uptake increases with decreasing RE ionic radius [37]. The enthalpy of proton migration for these compounds decreases for a bigger ionic radius. That is in accordance with the conductivity data for these compounds – the observed conductivity is lower for the larger rare-earth cation. Therefore, we suggest that the size and the content of yttrium apart from transport- may influence also the thermal properties of $Y_{2+x}Ti_{2-2x}Nb_xO_7$. In our previous work we have shown that in the $Y_3Nb_{1-x}Ti_xO_{7-\delta}$ system, the hydration was higher in samples with larger Ti content [10] since titanium in yttrium niobate was an acceptor-type substitution causing the increase of oxygen vacancies. That implies that not only the structure but also the cation composition itself may influence the hydration process and protonic defect concentration in fluorite-pyrochlore systems.

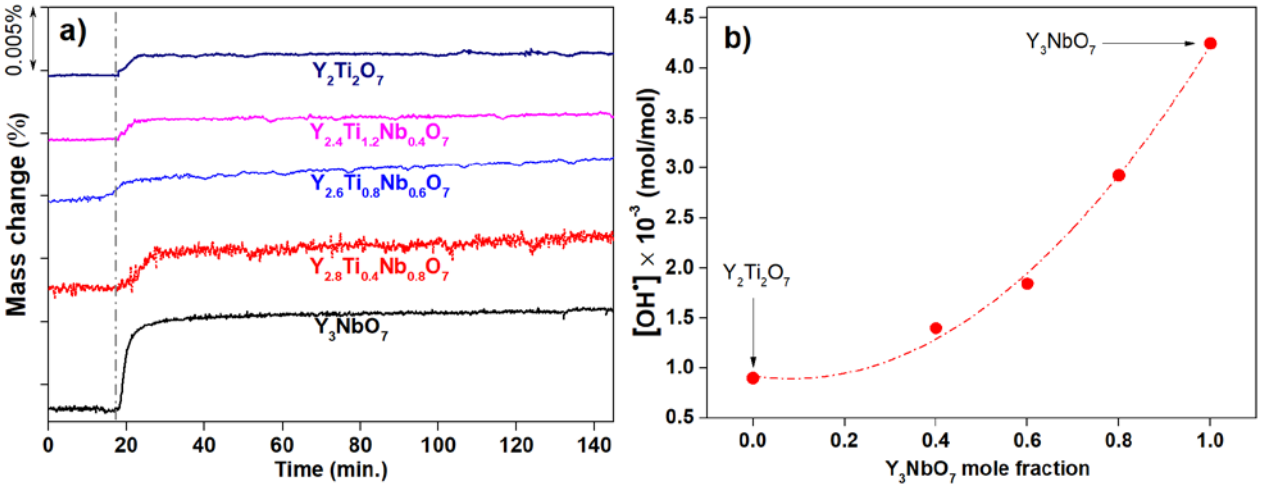

Figure 3 a) Thermograms of investigated samples under the isothermal switch between dry and wet gas. b) protonic defect concentration vs Y_3NbO_7 mole fraction.

Figure 4 shows the enthalpy of drop solution and the enthalpy of formation from oxides versus Y_3NbO_7 content. The enthalpy of formation was calculated using the thermodynamic cycles presented in Table 1. The drop solution enthalpy of all compounds, the enthalpy of formation from oxides, and the enthalpy of mixing of the $Y_{2+x}Ti_{2-2x}Nb_xO_7$ are summarized in Table 2. The enthalpies of mixing in the solid solution system are calculated as the difference between the drop solution enthalpies of the solid solution and the weighted average of the end-members.

Table 1 Thermodynamic cycles used to determine the enthalpies of formation from oxides.

$Y_{2+x}Ti_{2-2x}Nb_xO_7$ (s, 25 °C) → (2+x)/2 Y_2O_3 (dis, 800 °C) + (2-2x) TiO_2 (dis, 800 °C) + xNb_2O_5 (dis, 800 °C)	ΔH_{ds}
Y_2O_3 (s, 25 °C) → Y_2O_3 (dis, 800 °C)	ΔH_2
TiO_2 (g, 25 °C) → TiO_2 (dis, 800 °C)	ΔH_3
Nb_2O_5 (g, 25 °C) → Nb_2O_5 (dis, 800 °C)	ΔH_4
(2+x)/2 Y_2O_3 (s, 25 °C) + (2-2x) TiO_2 (s, 25 °C) + xNb_2O_5 (s, 25 °C) → $Y_{2+x}Ti_{2-2x}Nb_xO_7$ (s, 25 °C)	$\Delta H_{f,ox}$
$\Delta H_{f,ox} = -\Delta H_{ds} + (2+x)/2\Delta H_2 + (2-2x)\Delta H_3 + y\Delta H_4$	

Table 2 Average drop solution enthalpies at 800 °C for all compounds and their constituent oxides; enthalpies of formation from oxides ($\Delta H_{f,ox}$) and enthalpies of mixing of $Y_{2+x}Ti_{2-2x}Nb_xO_7$. Uncertainties are two standard deviations of the mean.

Compound	Structure	ΔH_{ds} kJ/mol	$\Delta H_{f,ox}$ kJ/mol	ΔH_{mix} kJ/mol
$Y_2Ti_2O_7$	*Fd-3m*	134.28 ± 1.27	-103.84 ± 1.89	0
$Y_{2.1}Ti_{1.8}Nb_{0.1}O_7$	*Fd-3m*	118.84 ± 1.34	-102.51 ± 1.95	-21.06 ± 3.12
$Y_{2.2}Ti_{1.6}Nb_{0.2}O_7$	*Fd-3m*	101.25 ± 0.61	-99.04 ± 1.57	-25.87 ± 2.54
$Y_{2.3}Ti_{1.4}Nb_{0.3}O_7$	*Fd-3m*	82.71 ± 1.01	-94.61 ± 1.79	-19.81 ± 2.23
$Y_{2.4}Ti_{1.2}Nb_{0.4}O_7$	*Fd-3m*	71.53 ± 0.88	-97.55 ± 1.75	-14.08 ± 2.12
$Y_{2.5}Ti_{1.0}Nb_{0.5}O_7$	*Fm-3m*	66.09 ± 0.94	-106.22 ± 1.82	-12.04 ± 1.91
$Y_{2.6}Ti_{0.8}Nb_{0.6}O_7$	*Fm-3m*	52.09 ± 0.92	-106.33 ± 1.82	-1.43 ± 1.69
$Y_{2.7}Ti_{0.6}Nb_{0.7}O_7$	*Fm-3m*	41.77 ± 0.47	-110.13 ± 1.72	3.44 ± 1.63
$Y_{2.8}Ti_{0.4}Nb_{0.8}O_7$	*Fm-3m*	31.79 ± 0.59	-114.26 ± 1.81	0.94 ± 1.34
$Y_{2.9}Ti_{0.2}Nb_{0.9}O_7$	*Fm-3m*	10.93 ± 1.45	-107.52 ± 2.29	-0.61 ± 1.79
Y_3NbO_7[b]	*Fm-3m*	-26.17 ± 3.07	-84.53 ± 3.45	0
Y_2O_3[38]		-116.30 ± 1.20		
TiO_2		73.37 ± 0.36		
Nb_2O_5[39]		127.50 ± 0.80		

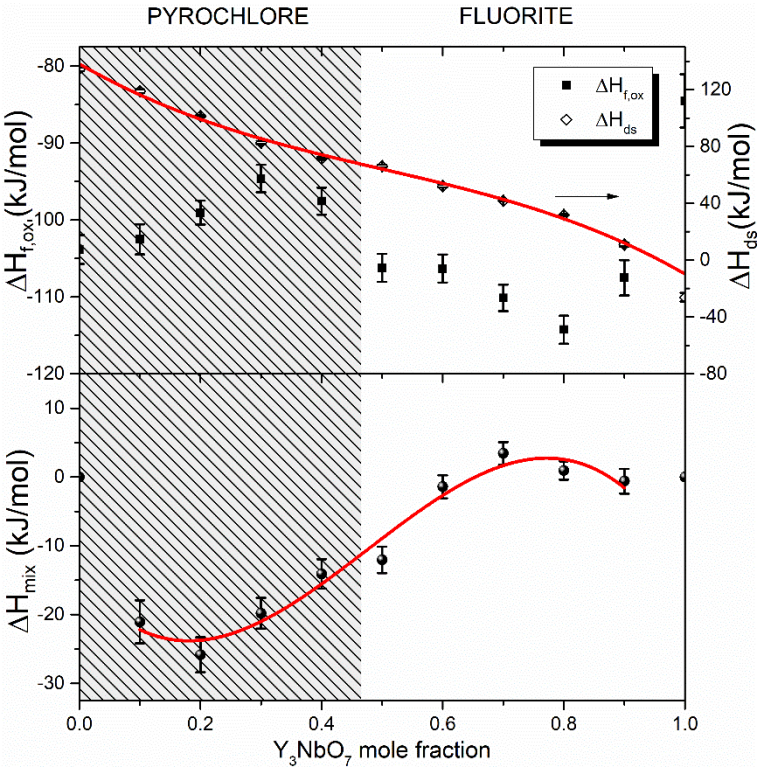

Figure 4 Enthalpies of drop solution and formation from binary oxides (top), enthalpies of mixing (bottom) of Y_3NbO_7 - $Y_2Ti_2O_7$ solid solutions. The error is two standard deviations of the mean. The line represents the 3rd degree polynomial fit of the achieved data.

Figure 4 presents the energetics of formation and mixing of investigated solid solutions. The measured $\Delta H_{f,ox}$ is strongly exothermic for all compositions, which means thermodynamic stability with respect to their binary oxides. For 8-fold coordination, the ionic radii of Nb^{5+} and Ti^{4+} are the same, therefore size difference would produce only small changes in the energetics of formation. Bigger changes are observed with changing sample structure. Such relationships have been observed previously for rare earth niobates[40]. In the present system, a linear change of formation enthalpy with increasing with changing the mole fraction of Y_3NbO_7 is observed in the enthalpies of formation from oxides, even though the structure changes from $Y_2Ti_2O_7$ pyrochlore to defect fluorite for Y_3NbO_7 [38]. The changes in the values of enthalpy of formation from oxides for investigated solid solutions can be attributed to a slightly less stable pyrochlore structure, then while the system becomes defect-fluorite structure. The enthalpy becomes the most exothermic reaching the minimum for x = 0.8. This suggests the greatest stability at that composition.

The heats of drop solution are presented in Table 2. Their values depend on the mole fraction of Y_3NbO_7, thus it is possible to calculate the quantitative enthalpy of mixing of this system. Enthalpy of mixing of the Y_3NbO_7 - $Y_2Ti_2O_7$ solid solutions is presented in Fig. 4 against the mole fraction of Y_3NbO_7. It has been shown that the positive heat of mixing is associated with cation size mismatch [41], as quantified by Davies and Navrotsky for a variety of oxide systems [38]. Considering the complete solution observed via X-ray diffraction, the mismatch induced by small cation ionic radius difference will produce close to zero heat of mixing. The subregular solution model (3rd degree of polynomial) has been used to fit pyrochlore and fluorite phase solid solutions separately due to differences in enthalpy of mixing being small positive for fluorite phases containing higher amounts of niobate phase. We can fit the whole range of compositions with one 3rd degree polynomial fit, which is in line with the structural data showing no abrupt changes while the structure changes. From the other point of view, almost zero or small positive heats of mixing for the compositions with disordered defect fluorite structure (x = 0.5 to 1.0) indicate that these compositions are energetically less stable as single-phase than the physical mixture of their end members. The X-ray diffraction results in the present study have shown additional weak reflections around 38 and 47 ° in the compositions with x = 0.5 to 0.8, suggesting local ordering. The heats of mixing also can suggest the presence of two phases at the nanoscale. Since the additional weak reflections could not be refined with either pyrochlore or defect fluorite structure, the local ordering may occur with two different fluorite related ordered structures e.g. pyrochlore microdomains [9]. Such two-phase pyrochlore and/or weberite-type ordered domains at nanoscale have been observed in the solid solution between fluorite related $Ho_2Ti_2O_7$ and $Ho_2Zr_2O_7$ oxides [42, 43]. Neutron diffraction experiments and pair distribution function analysis of $Y_2Ti_2O_7$-Y_3NbO_7 solid solutions would give further understandings of the structure on different length scales .

A representative complex impedance plot is presented for $Y_{2.9}Ti_{0.2}Nb_{0.9}O_7$ in Fig.5. Two separate semicircles may be distinguished, which can be described by an R(RQ)(RQ) equivalent circuit (expressed in Circuit Description Code [44]). The constant phase element Q depends on the impedance according to the formula $Z^{-1} = Y = Q_0 \cdot (i\omega)^n$, where the admittance Q_0 and the angle of misalignment, n, are the fitted parameters. From these parameters and the measured resistance, pseudo-capacitances C were calculated for each semicircle by using the equation (4):

$$C = Q^{\frac{1}{n}} R^{\left(\frac{1}{n} - 1\right)} \tag{4}$$

The first (RQ) element, representing the semicircle observed for higher frequencies, has capacitance in the order of magnitude around 10^{-11} F·cm^{-1} which reflects the bulk conduction processes. The other semicircle at lower frequencies, which capacitance is around 10^{-7} F·cm^{-1}, may be attributed to electrode response [45]. Therefore, only the response associated with bulk conductivity has been analyzed.

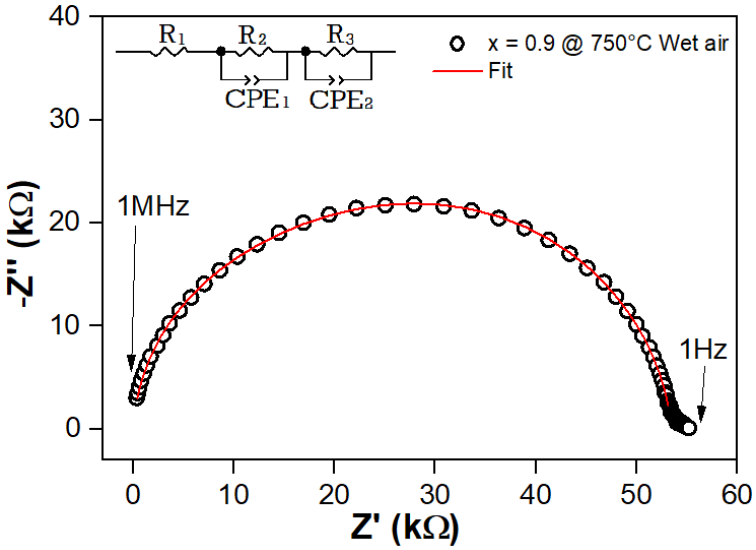

Figure 5 Typical complex impedance data (open symbols) with the fit (line) and corresponding equivalent circuit exemplified for $Y_{2.9}Ti_{0.2}Nb_{0.9}O_7$.

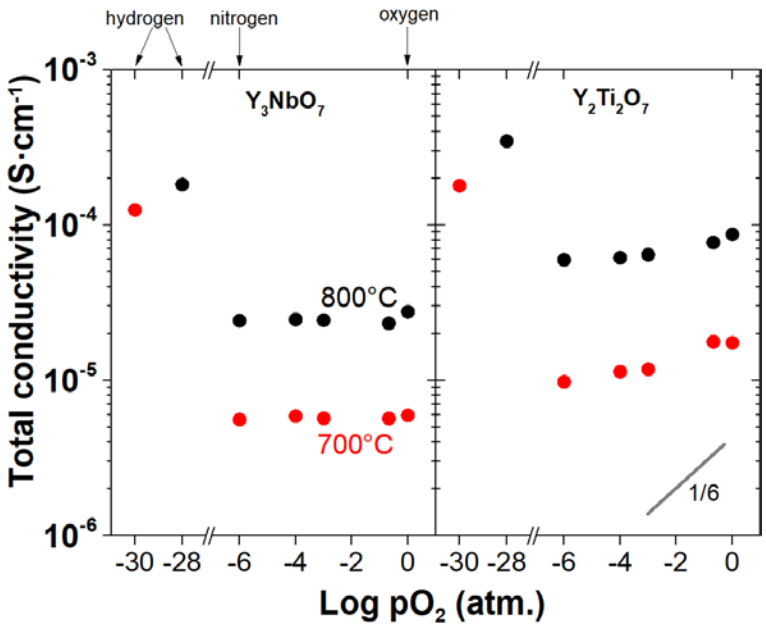

Figure 6 Total conductivity as a function of oxygen partial pressure. The black line with 1/6 slope illustrates the model case with interstitial oxygens O_i'' compensated with holes $h^{\bullet}$.

Total conductivity measured as a function of oxygen partial pressure in dry atmospheres is presented in Fig. 6. The results show that conductivity of Y_3NbO_7 is virtually independent of the pressure at high oxygen partial pressures (from 10^{-6} to 10^{-1} atm.). Only the conductivity in O_2 (pressure 10^0 atm.) at 800 °C is slightly higher. This indicates that material is oxygen ion conductor in this pO_2 region, while as the pressure increases, and exceeds 1 bar of O_2, p-type conductivity may become dominant [46]. These findings adhere well to results from the literature. For instance, the mean square displacement calculations of ions in Y_3NbO_7 performed by Norberg clearly show that oxygen ions are mobile, whilst cations present no diffusive behavior [47]. Another interesting observation from that work is that in yttrium niobate only a small number of oxygen ions are mobile, whereas the others almost do not take part in conduction. This explains the low values of conductivity observed in the measurement and implies a tightly bonded structure.

A different situation is observed in $Y_2Ti_2O_7$, where the conductivity increases with oxygen pressure, which indicates partial hole conductivity. This confirms the expectations since the electron hole hopping between Ti^{3+} and Ti^{4+} cations is rather typical conductivity mechanism of

titanates [48, 49]. The most probable reaction occurring in $Y_2Ti_2O_7$ in oxidizing atmospheres is that the excess oxygen ions occupy the interstitial positions, following equation:

$$\frac{1}{2}O_{2(g)} = O_i'' + 2h^{\bullet} \quad (5)$$

The negatively charged oxygen ions are compensated by electron holes, increasing p-type partial conductivity, however, the conductivity dependence has much smaller slope than 1/6. We believe this is a transition region between ionic- and p-type electronic conduction mechanism and we expect the slope of 1/6 in higher pO_2.

In hydrogen, both yttrium niobate and yttrium titanate exhibit total conductivity one order of magnitude higher than in the intermediate range of pO_2. The reaction which probably dominates in low pO_2 region is the reduction of oxygen species:

$$O_O^X = v_O^{\bullet\bullet} + 2e' + \frac{1}{2}O_{2(g)} \quad (6)$$

Therefore the charge compensation rule causes two electrons to be generated for each reduced oxygen, giving a noticeable rise in total conductivity. This indicates that n-type conductivity dominates in hydrogen atmosphere.

So far, $\sigma(pO_2)$ dependencies for yttrium niobates and titanates have been reported only for Y_3NbO_7 [37], $Y_{0.8}Nb_{0.2}O_{1.7}$ [50] and $Y_2Ti_2O_7$ [51–53]. In the case of $Y_{2+x}Zr_{2-2x}Nb_xO_7$ solid solutions, the conductivity dependence on oxygen partial pressure varied for different samples [54]. In these compounds, for low-yttria pyrochlores (x = 0.2, x = 0.3 and x = 0.4) , the conductivity is oxygen-ion type, whereas, for cubic fluorite samples (x = 0.6, x = 0.8 and x = 1), the n-type conductivity surpasses the ionic conductivity between 10^{-14} and 10^{-8} Pa. End members exhibit electronic conductivity in reducing atmospheres, and yttrium titanate also exhibits p-type conductivity in pure oxygen. In similar ternary systems consisting of ZrO_2-Y_2O_3-TiO_2, increasing yttrium content provides slightly higher electronic and significantly lower ionic conductivity [55, 56]. For $Y_{0.2}Ti_{0.18}Zr_{0.62}O_{1.9}$ at 930 °C, the highest electronic conductivity $2 \cdot 10^{-1} S \cdot cm^{-1}$ was reported [55]. Moreover, the dependence of total conductivity on oxygen partial pressure was similar to that observed in Y_3NbO_7 and $Y_2Ti_2O_7$ – c.f. Fig.6.

The total conductivities as a function of temperature for selected samples, measured in dry/wet air and dry/wet hydrogen atmospheres are shown in Figs. 7 and 8, respectively.

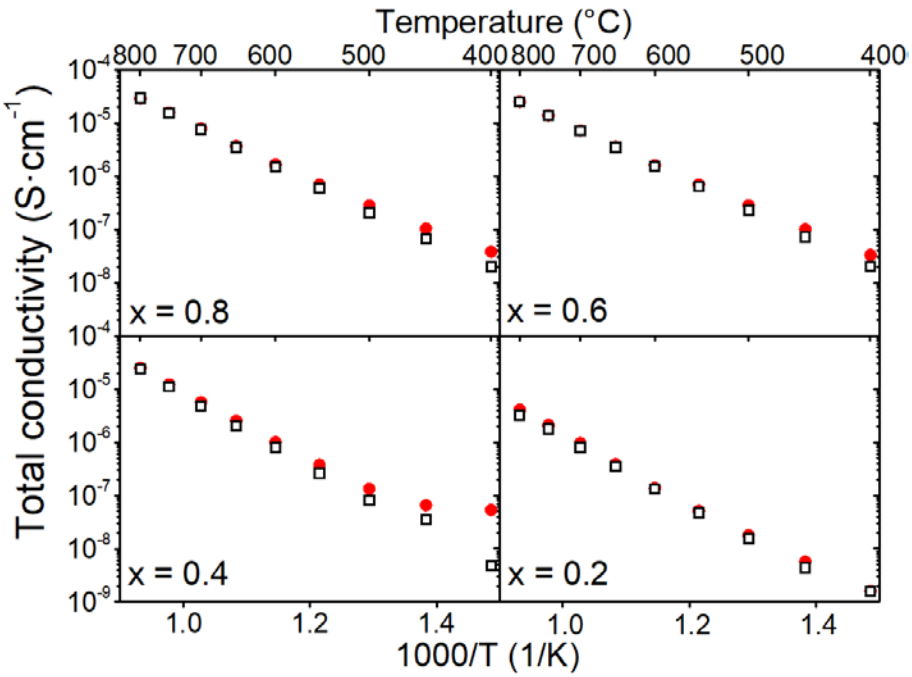

Figure 7 Total conductivity as a function of inverse temperature for $Y_{2+x}Ti_{2-2x}Nb_xO_7$ samples, collected in dry air (open squares) and wet air (red circles)

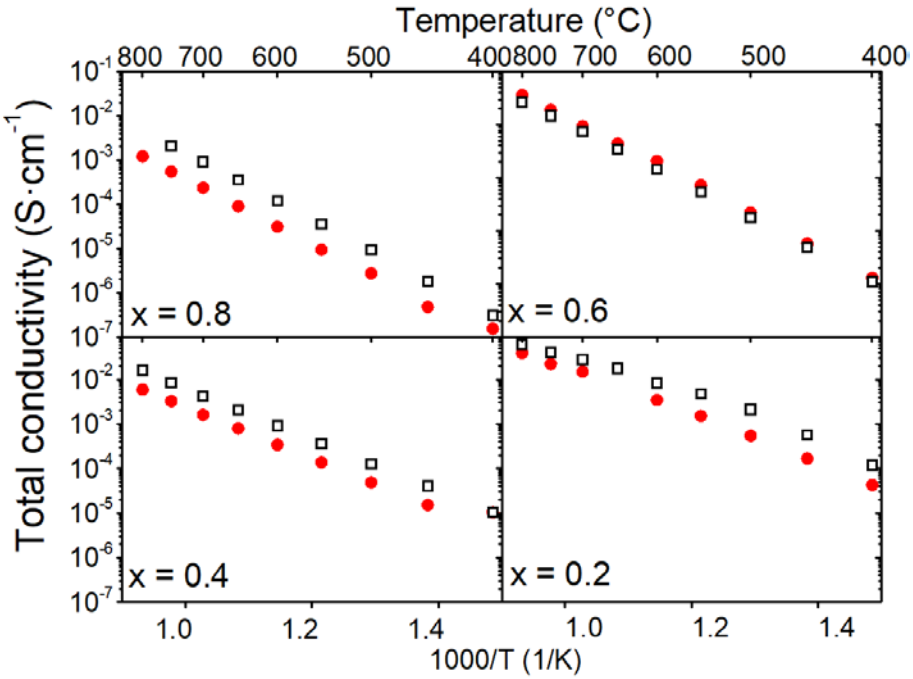

Figure 8 Total conductivity as a function of inverse temperature for $Y_{2+x}Ti_{2-2x}Nb_xO_7$ samples, collected in dry hydrogen (open squares) and wet hydrogen (red circles)

Generally, the conductivities of yttrium niobate and yttrium titanate are relatively low. In all cases, the total conductivity is higher in wet than it is in dry air. For example, for x = 0.4 at 500 °C, conductivity is 8.08×10^{-8} S·cm^{-1} in dry air and 1.33×10^{-7} S·cm^{-1} in wet air. The maximum conductivity in the air at 800 °C is observed for $Y_{2.9}Ti_{0.2}Nb_{0.9}O_7$ and equals to 3.02×10^{-5} S·cm^{-1}. Higher total conductivity in wet air suggests that mobile protonic defects are present, as hinted by thermogravimetric data – (see Fig. 3a, b). The activation energies (Tab.3) were calculated from the Arrhenius type conductivity equation in higher (600 – 800 °C) and lower (400 – 550 °C) temperature ranges.

Table 3 Activation energies E_A at higher and lower temperatures in air and hydrogen with total conductivity σ at 600°C in air and hydrogen

Sample	E_A (eV) 600 – 800°C		E_A (eV) 400 – 550°C		$\sigma \cdot 10^{-6}$ ($S \cdot cm^{-1}$) 600°C	E_A (eV) 600 – 800°C		E_A (eV) 400 – 550°C		$\sigma \cdot 10^{-5}$ ($S \cdot cm^{-1}$) 600°C
	Wet air	Dry air	Wet air	Dry air	Dry air	Wet H_2	Dry H_2	Wet H_2	Dry H_2	Dry H_2
Y_3NbO_7	1.31(1)	1.39(1)	0.94(5)	1.17(4)	1.05(1)	1.73(2)	1.83(2)	0.85(4)	0.96(5)	0.18(1)
$Y_{2.9}Ti_{0.2}Nb_{0.9}O_7$	1.31(1)	1.36(1)	0.99(4)	1.19(3)	1.28(1)	1.61(1)	1.56(4)	1.38(4)	1.64(1)	5.8(3)
$Y_{2.8}Ti_{0.4}Nb_{0.8}O_7$	1.24(1)	1.29(1)	0.99(3)	1.15(3)	1.48(1)	1.56(1)	1.55(2)	1.4(1)	1.59(1)	11.9(6)
$Y_{2.7}Ti_{0.6}Nb_{0.7}O_7$	1.20(1)	1.23(1)	1.00(2)	1.19(1)	0.88(1)	1.36(2)	1.35(2)	1.33(2)	1.39(2)	1.99(1)
$Y_{2.6}Ti_{0.8}Nb_{0.6}O_7$	1.20(1)	1.21(1)	1.04(2)	1.16(1)	1.54(1)	1.27(1)	1.24(3)	1.31(1)	1.34(1)	14.4(7)
$Y_{2.5}Ti_{1.0}Nb_{0.5}O_7$	1.18(1)	1.19(1)	1.06(1)	1.18(1)	0.78(1)	1.16(2)	1.17(3)	1.23(1)	1.27(1)	28.6(1)
$Y_{2.4}Ti_{1.2}Nb_{0.4}O_7$	1.38(1)	1.46(2)	1.0(1)	1.3(1)	0.80(1)	1.24(1)	1.24(2)	0.9(2)	1.19(1)	91.5(5)
$Y_{2.3}Ti_{1.4}Nb_{0.3}O_7$	1.42(1)	1.50(3)	1.27(6)	1.2(2)	0.51(1)	1.11(1)	1.09(2)	1.13(1)	1.11(1)	158(16)
$Y_{2.2}Ti_{1.6}Nb_{0.2}O_7$	1.39(2)	1.46(2)	1.16(8)	1.17(2)	0.13(1)	1.05(6)	0.87(5)	1.20(1)	1.25(8)	827(1)
$Y_{2.1}Ti_{1.8}Nb_{0.1}O_7$	1.50(5)	1.78(9)	0.7(1)	1.06(4)	0.37(1)	0.96(1)	0.89(1)	1.09(1)	1.02(2)	337(1)
$Y_2Ti_2O_7$	1.42(1)	1.45(1)	1.05(3)	1.23(5)	6.43(1)	1.47(2)	1.3(1)	1.0(1)	1.61(4)	2.00(1)

The influence of temperature and atmosphere on activation energies of conductivity is not straightforward. In the lower temperature range, the activation energy is higher in dry atmosphere for the majority of the samples, while at high temperatures it is opposite. This suggests that two different mechanisms of conduction may dominate in the low- and high-temperature ranges. Interestingly, the activation energies are much higher than for typical ionic conductors [57–61] (related both to oxygen ionic and protonic conductivity). This indicates that either the energy barrier for mobility is high (i.e. enthalpy of mobility) or the enthalpy of defect formation is high, or both. In either case, it indicates a strongly bonded and stable structure. Moreover, this is also supported by the low values of total conductivity itself. These findings may be connected with the strongly exothermic enthalpies of formation of yttrium niobate and titanate, that is, -84.6 kJ/mol and -103.84 kJ/mol, respectively, [38] which suggests their strongly bonded crystal structure and low mobility of ions. It has been shown for multiple fluorite systems that oxygen conductivity is strongly correlated with the enthalpy of formation from binary oxides[62–64]. For example, in rare-earth-doped ceria systems, Avila-Paredes et al. have shown the correlation

between the maximum of ionic conductivity and maximum of enthalpy of formation which indicates destabilization of this system[65]. For the thoria system, a similar relationship has been reported, where the formation enthalpy from oxides is positive over the composition range and a maximum is observed at 0.23 mol fraction of $LaO_{1.5}$ and 0.13 mol fraction of $YO_{1.5}$. The reported position of the conductivity maximum varies between 0.12 and 0.14 mol fraction of $YO_{1.5}$ and is close to measured enthalpy maximum[64]. Similar behavior has been observed also for proton conductors, e.g. the barium zirconate system[66].

The total conductivities of $Y_{2+x}Ti_{2-2x}Nb_xO_7$ solid solutions at each temperature vary by two orders of magnitude for different x values. Another observation is that the total conductivity and activation energies exhibit non-monotonic change with x. Similar characteristics were found by Norberg et al. in the $Y_2(Ti_{1-x}Zr_x)_2O_7$ system[67]. They postulated that larger x leads to an increase in the degree of disorder within the anion sublattice thus increasing the ionic conductivity. On the other hand, Marrocchelli et al. [15] found that, in the $(Y_3NbO_7)_x(Y_2Zr_2O_7)_{1-x}$ solid solution, increasing content of Nb^{5+} ions, by introducing strain into the cation sublattice, increases the tendency of oxygen ion trapping, which decreases the ion mobility. The observed non-monotonic dependence of total conductivity on x in $Y_{2+x}Ti_{2-2x}Nb_xO_7$ solid solutions may be related to the competition between these two effects.

The total conductivities in solid solution samples are noticeably higher in hydrogen than in air (cf. Figs 7 and 8). For instance, in $Y_{2.2}Ti_{1.6}Nb_{0.2}O_7$ at 600 °C, the conductivity in dry hydrogen is almost five orders of magnitude higher than in dry air. This significant difference is probably caused by the electronic contribution originating from reduced oxygen species, which overcomes the ionic part. In general, the conductivities in hydrogen are higher in samples with higher titanium content. However, in this atmosphere, $Y_2Ti_2O_7$ conductivity is not as high as in other examined pyrochlores (see. Table 3). The relationship between the structural ordering in the crystal structure and the electrical properties was discussed previously for similar Y- Zr-Nb ternary systems and their solid solutions. In $Y_{2+x}Zr_{2-2x}Nb_xO_7$ [47] and $Y_{0.6+2.4x}Zr_{3.4-3.4x}Nb_xO_{7.72-0.72x}$ [54] the total conductivity decreases with increasing *x*. On the other hand, in $Y_{2+x}Ti_{2-2x}Nb_xO_7$ system investigated by us, the total conductivity changes non-monotonically with *x*, however the defect fluorite end member (x = 1) exhibits lower conductivity in air and hydrogen than the pyrochlore end member (x = 0), like in $Y_{2+x}Zr_{2-2x}Nb_xO_7$ and

$Y_{0.6+2.4x}Zr_{3.4-3.4x}Nb_xO_{7.72-0.72x}$. In the temperature range between 600 and 800 °C the activation energies of the total conductivity in wet hydrogen atmosphere exceed those in dry H_2. This suggests that electronic contribution is higher than protonic contribution to the total conductivity. However, we cannot clearly exclude the proton conductivity in hydrogen, since in lower temperature range (400 – 550°C) in almost every case the activation energies are lower in wet H_2.

To analyze the relations between different charge carriers in the total conductivity in different materials and temperature regions, the ratios of conductivities in dry hydrogen and air are plotted in Fig. 9.

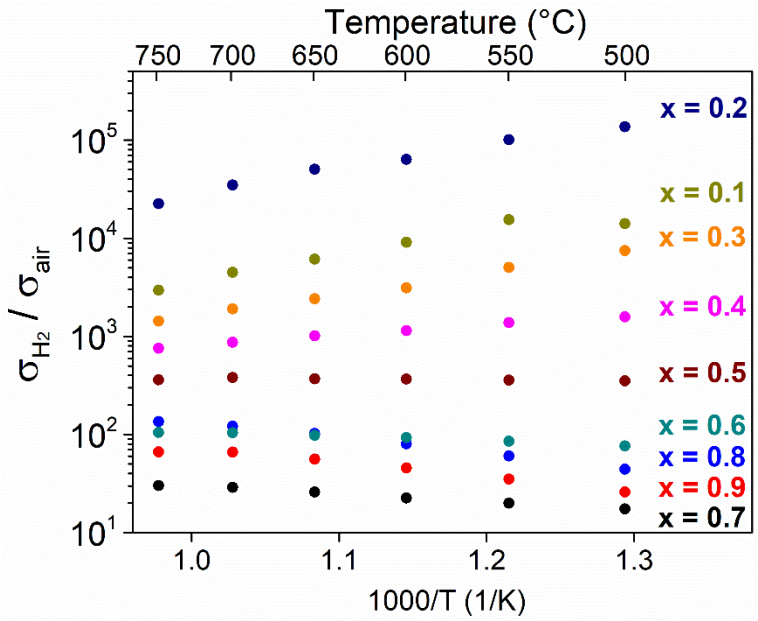

Figure 9 Temperature dependence of the ratio of conductivity in dry hydrogen and dry air for the solid solutions with different Y_3NbO_7 mole fractions (x).

Similar characteristics have been obtained for humidified atmospheres. It can be seen that the Y_3NbO_7 mole fraction (x) influences the conductivity ratio as well as the temperature dependence. The protonic conductivity for investigated solid solutions is relatively small, hence the ratio of conductivities depends mainly on the relation between the oxygen ion - and electronic conductivity. As can be seen, the ratio of conductivities is higher in the pyrochlore samples than in defect-fluorites. What is interesting, for $Y_{2.5}Ti_{1.0}Nb_{0.5}O_7$, i.e. the sample with equimolar contents of yttrium niobate and titanate, the slope of the temperature dependence of conductivity ratio is almost zero. Therefore, in this compound, the contributions of the oxygen ion and

electronic conductivities do not vary with temperature. In this case, the conductivity in hydrogen is around 400 times higher than in air. For samples with lower titanium content, the ratio increases with increasing temperature. For samples where $x < 0.5$, the conductivity ratio decreases with increasing temperature. These relations depend on the activation energy in air and in hydrogen. The activation energy depends on the enthalpies of mobility of dominating charge carriers, namely the electrons in reducing, and oxygen ions in oxidizing atmospheres and in the intermediate range of pO_2. Therefore the changes in slope for $x < 0.5$ and $x > 0.5$ result from the contribution of electronic part of conductivity, which is higher in samples with more titanium content. On the other hand, for samples where niobium content is larger than 0.5, the total conductivity in dry air is higher than in dry hydrogen, which suggests that the ionic part in these samples overcomes the electronic. As can be seen from Fig. 9, the slope of the temperature dependence of conductivity ratio between 550 and 750 °C is the steepest for $x = 0.1$, and $x = 0.8$, which shows that for these samples, the enthalpies of mobility in hydrogen differ the most from the enthalpies of mobility in air, compared with other samples. It is interesting that the $Y_{2+x}Ti_{2-2x}Nb_xO_7$ end members do not match the trend shown by the other samples. The ratio of conductivities merely exceeds 5 and 4 for yttrium niobate and yttrium titanate, respectively For these samples, the slope of the conductivity ratio vs temperature is non-monotonic. This indicates that not only the yttrium content, which occupies A-site in $Y_{2+x}Ti_{2-2x}Nb_xO_7$ solid solutions, but also the Nb/Ti cations, which substitute each other on B-site, influence the conduction mechanism in oxidizing and reducing atmospheres. Moreover, niobium and titanium for 8-fold coordination have the same ionic radius, hence it may be stated that the ionic radii do not significantly influence the electrical properties of the investigated system.

Protonic conductivity was an important part of this study. To further analyze it, we have estimated the contribution of protons to total conductivity using the following formula $\frac{\sigma_{wet}-\sigma_{dry}}{\sigma_{wet}}$, where σ_{wet} and σ_{dry} denote total conductivity measured in wet and dry air, respectively. This can be done only for materials for which in dry conditions electrical conductivity is dominated by oxygen ion transport and in which the hydration reaction dominates in wet atmospheres. In yttrium titanate the conductivity at $pO_2 = 10^0$ atm. is higher than that at intermediate oxygen partial pressures hence this material showed hole conductivity in air, while yttrium niobate did not (cf. Fig. 6). Considerable water uptake is observed only for the samples with higher

Nb contents (cf. Figs.3a,b). Therefore, protonic conductivity estimations were performed only for high Nb-content specimens ($x \geq 0.5$). Fig. 10 shows the estimated relative protonic contribution. The values increase with Y_3NbO_7 mole fraction and are higher at lower temperatures. Generally, for oxides exhibiting protonic conductivity like in $Y_{2+x}Ti_{2-2x}Nb_xO_7$, the protonic contribution to total conductivity is higher at lower temperatures (cf. Fig.7). The mobility and concentration of protonic species are a function of temperature, and with decreasing temperature, the increasing concentration greatly overcomes the decreasing mobility [68]. In effect, the protonic conductivity goes through a maximum as a function of temperature. On the other hand, in pyrochlore samples, for $x < 0.5$, the total conductivity is also higher in wet than in dry air, however, no strict dependence of relative protonic contribution was found.

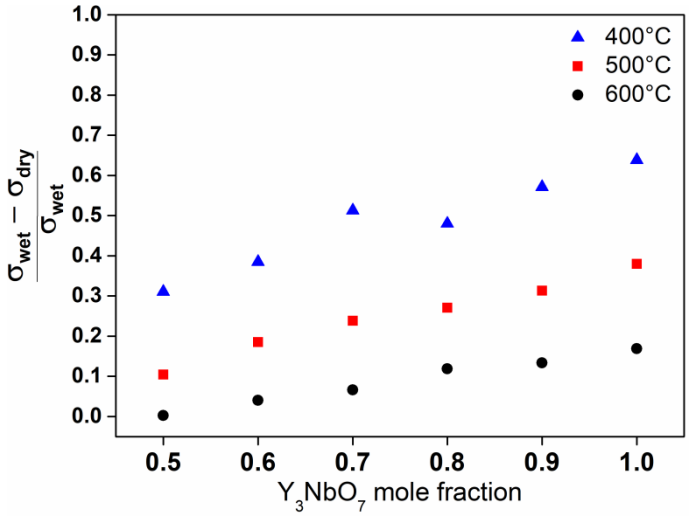

Figure 10 $\frac{\sigma_{wet}-\sigma_{dry}}{\sigma_{wet}}$ ratio vs Y_3NbO_7 mole fraction (x) for samples with $x \geq 0.5$.

In our previous work on $Y_3Nb_{1-x}Ti_xO_{7-\delta}$ the water uptake, as well as protonic defect concentration, were both higher for the samples with higher Ti content[10]. The opposite trend is observed in the $Y_{2+x}Ti_{2-2x}Nb_xO_7$ solid solutions, where higher Ti content yields lower protonic contribution. In these compounds, however, the role of titanium is different from that in $Y_3Nb_{1-x}Ti_xO_{7-\delta}$. It is not an acceptor-type constituent, therefore in the $Y_{2+x}Ti_{2-2x}Nb_xO_7$ solid solutions only intrinsic defects are present, the concentration of which is typically orders of magnitude lower than in doped systems. Therefore, the Ti/Nb ratio affects protonic conductivity differently. Three possible factors related to the Y_3NbO_7 mole fraction (x) can affect the protonic contribution:

I. Structural changes, from pyrochlore to defect fluorite, enforced by changing Nb content.

II. Decreasing hole concentration, which is detrimental to proton incorporation due to hole-proton interactions[69], as the Ti content decreases.

III. Chemical properties of the cations themselves, e.g. electronegativity or ionic radii of Ti and Nb, which influence chemical bonding and stability of protonic defects [70, 71].

At this stage, it can be hypothesized that either the first or the second or both factors are relevant for the protonic conductivity changes with x. The third one is unlikely since in these compounds ionic radii of Ti^{4+} and Nb^{5+} are the same and the electronegativity of the elements is almost identical.

Conclusions

The solid solutions of defect-fluorite Y_3NbO_7 and pyrochlore $Y_2Ti_2O_7$ were synthesized via a solid-state reaction method. The resulting stoichiometry of the compounds is $Y_{2+x}Ti_{2-2x}Nb_xO_7$, where $0 \leq x \leq 1$. All of the samples were single-phase, however, in a few defect-fluorite samples, additional pyrochlore ordering was present in the structure, which may be attributed to pyrochlore nanodomain formation. Each of the examined materials hydrate in humidified atmosphere at 300 °C. The estimated protonic defect concentration increases with *x*, exceeding $4.0 \cdot 10^{-3}$ mol/mol for Y_3NbO_7. All investigated compositions exhibit strongly exothermic enthalpies of formation from binary oxides and negative or close to zero enthalpies of mixing which confirm that the crystal structure is tightly bonded. Solid solution end members are oxygen ion conductors, exhibiting electronic conductivity in hydrogen, where conductivities are a few orders of magnitude higher than in air. The temperature-dependent ratio of conductivity in hydrogen and air was found, suggesting that not the yttrium, but rather the Nb/Ti content is crucial in the conduction mechanism, and ionic radii do not show significant influence on total conductivity. For $x < 0.5$ and $x > 0.5$, The changes in slope in the ratio of conductivities result from enthalpies of mobility of major charge carriers which dominate in reducing or oxidizing atmospheres. The calculated $\frac{\sigma_{wet}-\sigma_{dry}}{\sigma_{wet}}$ conductivity ratio increases with decreasing temperature suggesting that protonic species are more dominant at lower temperatures, because of their

concentration. What is more, in defect fluorite samples ($x \geq 0.5$) the protonic conductivity is predominant in wet air.

Acknowledgments

This work was partially supported by project no. 2016/23/B/ST5/02137 founded by the National Science Centre, Poland.

The calorimetric studies were supported by the U.S. Department of Energy Office of Basic Energy Science, grant DE-FG02-03ER46053.

References

1. Jaffe B, Roth RS, Marzullo S. Piezoelectric properties of Lead zirconate-Lead titanate solid-solution ceramics. *J Appl Phys*. 1954; 25(6): 809–810. https://doi.org/10.1063/1.1721741

2. Ozawa M. Role of cerium-zirconium mixed oxides as catalysts for car pollution: A short review. *J Alloys Compd*. 1998; 275–277: 886–890. https://doi.org/10.1016/S0925-8388(98)00477-0

3. Perry NH, Kim N, Ertekin E, Tuller HL. Origins and Control of Optical Absorption in a Nondilute Oxide Solid Solution: $Sr(Ti,Fe)O_{3-x}$ Perovskite Case Study. *Chem Mater*. 2019;31(3):1030–1041. https://doi.org/10.1021/acs.chemmater.8b04580

4. Iwahara H, Yajima T, Hibino T, Ozaki K, Suzuki H. Protonic conduction in calcium, strontium and barium zirconates. *Solid State Ionics*. 1993;61(1):65–69. https://doi.org/10.1016/0167-2738(93)90335-Z

5. Caetano E, De Souza C, Muccillo R, Souza ECC de, Muccillo R. Properties and applications of perovskite proton conductors. *Mater Res*. 2010;13(3):385–394. https://doi.org/10.1590/S1516-14392010000300018

6. Gdula-Kasica K, Mielewczyk-Gryn A, Lendze T, Molin S, Kusz B, Gazda M. Synthesis of acceptor-doped Ba-Ce-Zr-O perovskites. *Cryst Res Technol*. 2010;45(12):1251–1257. https://doi.org/10.1002/crat.201000380

7. Hume-Rothery W, Powell HM. On the Theory of Super-Lattice Structures in Alloys. *Zeitschrift für Krist - Cryst Mater*. 2014;91(1–6):23–47. https://doi.org/10.1524/zkri.1935.91.1.23

8. Shannon RD. Revised Effective Ionic Radii and Systematic Studies of Interatomie Distances in Halides and Chaleogenides. *Acta Cryst*. 1976;32.

9. López-Conesa L, Rebled JM, Chambrier MH, *et al*. Local Structure of Rare Earth Niobates (RE_3NbO_7, RE = Y, Er, Yb, Lu) for Proton Conduction Applications ⁂. *Fuel Cells*. 2013;13(1):29–33. https://doi.org/10.1002/fuce.201200136

10. Winiarz P, Mielewczyk-Gryń A, Wachowski S, Jasiński P, Witkowska A, Gazda M. Structural and electrical properties of titanium-doped yttrium niobate. *J Alloys Compd*. 2018;767:1186–1195. https://doi.org/10.1016/j.jallcom.2018.07.134

11. Singh BP, Parchur AK, Singh RK, Ansari AA, Singh P, Rai SB. Structural and up-conversion properties of Er^{3+} and Yb^{3+} co-doped $Y_2Ti_2O_7$ phosphors. *Phys Chem Chem Phys*. 2013;15(10):3480–3489. https://doi.org/10.1039/c2cp44195k

12. Rittman DR, Turner KM, Park S, *et al*. High-pressure behavior of $A_2B_2O_7$ pyrochlore (A=Eu, Dy; B=Ti, Zr). *J Appl Phys*. 2017;121(4). https://doi.org/10.1063/1.4974871

13. Momma K, Izumi F. VESTA 3 for three-dimensional visualization of crystal, volumetric and morphology data. *J Appl Crystallogr*. 2011;44:1272–1276. https://doi.org/https://doi.org/10.1107/S0021889811038970

14. Subramanian M a., Aravamudan G, Subba Rao GV. Oxide pyrochlores — A review. *Prog Solid State Chem*. 1983;15:55–143. https://doi.org/10.1016/0079-6786(83)90001-8

15. Marrocchelli D, Madden PA, Norberg ST, Hull S. Cation composition effects on oxide conductivity in the $Zr_2Y_2O_7$–Y_3NbO_7 system. *J Phys Condens Matter*. 2009;21(40):405403. https://doi.org/10.1088/0953-8984/21/40/405403

16. Li ZP, Mori T, Zou J, Drennan J. Optimization of ionic conductivity in solid electrolytes through dopant-dependent defect cluster analysis. *Phys Chem Chem Phys*. 2012;14(23):8369–8375. https://doi.org/10.1039/c2cp40845g

17. Holliday K, Finkeldei S, Neumeier S, Walther C, Bosbach D, Stumpf T. TRLFS of Eu^{3+} and Cm^{3+} doped $La_2Zr_2O_7$: A comparison of defect fluorite to pyrochlore structures. *J Nucl Mater*. 2013;433(1–3):479–485. https://doi.org/10.1016/j.jnucmat.2012.10.028

18. Xiao HY, Gao F, Weber WJ. Ab initio investigation of phase stability of $Y_2Ti_2O_7$ and $Y_2Zr_2O_7$ under high pressure. *Phys Rev B - Condens Matter Mater Phys*. 2009;80(21):1–4. https://doi.org/10.1103/PhysRevB.80.212102

19. Winiarz P. Structural and electrical properties of doped yttrium niobate and yttrium titanate, PhD Thesis. Gdansk University of Technology; 2019

20. Zinkevich M, Djurovic D, Aldinger F. Thermodynamic modelling of the cerium-oxygen system. *Solid State Ionics*. 2006;177(11–12):989–1001. https://doi.org/10.1016/j.ssi.2006.02.044

21. Maram PS, Ushakov S V., Weber RJK, Benmore CJ, Navrotsky A. Probing disorder in pyrochlore oxides using in situ synchrotron diffraction from levitated solids- A thermodynamic perspective. *Sci Rep*. 2018; 8(1): 1–11. https://doi.org/10.1038/s41598-018-28877-x

22. Rooksby HP, White EAD. Rare-Earth Niobates and TantaIates of Defect Fluorite- and Weberite-Type Structures. *J Am Ceram Soc*. 1964;47(2):94–96. https://doi.org/10.1111/j.1151-2916.1964.tb15663.x

23. Chtoun E, Hanebali L, Garnier P, Kiat JM. X-rays and neutrons rietveld analysis of the solid solutions (1-x)($A_2Ti_2O_7$)-x($MgTiO_3$) (A = Y or Eu). *Eur J Solid State Inorg Chem*. 1997;34:553–561.

24. Navrotsky A. Progress and New Directions in Calorimetry: A 2014 Perspective. *J Am Ceram Soc*. 2014;97(11):3349–3359. https://doi.org/10.1111/jace.13278

25. Reid DP, Stennett MC, Hyatt NC. The fluorite related modulated structures of the $Gd_2(Zr_{2-x}Ce_x)O_7$ solid solution: An analogue for Pu disposition. *J Solid State Chem*. 2012;191:2–9. https://doi.org/10.1016/j.jssc.2011.12.039

26. van Dijk MP, Mijlhoff FC, Burggraaf AJ. Pyrochlore microdomain formation in fluorite oxides. *J Solid State Chem*. 1986; 62(3): 377–385. https://doi.org/10.1016/0022-4596(86)90253-7

27. Liu Y, Withers RL, Norén L. The pyrochlore to “defect fluorite” transition in the $Y_2(Zr_yTi_{1-y})_2O_7$ system and its underlying crystal chemistry. *J Solid State Chem*. 2004;177(12):4404–4412. https://doi.org/10.1016/j.jssc.2004.09.014

28. Uehara T, Koto K, Kanamaru F, Horiuchi H. Stability and antiphase domain structure of the pyrochlore solid solution in the $ZrO_2Gd_2O_3$ system. *Solid State Ionics*. 1987; 23(1–2):137–143. https://doi.org/10.1016/0167-2738(87)90093-2

29. Gómez-Pérez A, Prado-Gonjal J, Muñoz-Gil D, *et al*. Anti-site disorder and physical properties in microwave synthesized $RE_2Ti_2O_7$ (RE = Gd, Ho) pyrochlores. *RSC Adv*. 2015;5(104):85229–85241. https://doi.org/10.1039/C5RA07796F

30. Løken A, Ricote S, Wachowski S. Thermal and Chemical Expansion in Proton Ceramic Electrolytes and Compatible Electrodes. *Crystals*. 2018; 8(9): 365. https://doi.org/10.3390/cryst8090365

31. Bishop SR, Marrocchelli D, Chatzichristodoulou C, *et al*. Chemical Expansion: Implications for Electrochemical Energy Storage and Conversion Devices. *Annu Rev Mater Res*. 2014;44(1):205–239. https://doi.org/10.1146/annurev-matsci-070813-113329

32. Yamazaki Y, Yang C-KK, Haile SM. Unraveling the defect chemistry and proton uptake of yttrium-doped barium zirconate. 2011 https://doi.org/10.1016/j.scriptamat.2010.12.034

33. Besikiotis V, Ricote S, Jensen MH, Norby T, Haugsrud R. Conductivity and hydration trends in disordered fluorite and pyrochlore oxides: A study on lanthanum cerate-zirconate based compounds. *Solid State Ionics*. 2012; 229: 26–32. https://doi.org/10.1016/j.ssi.2012.10.004

34. Mielewczyk-Gryń A, Wachowski S, Prześniak-Welenc M, *et al*. Water uptake analysis of the acceptor-doped lanthanum orthoniobates. *J Therm Anal Calorim*. 2019.

35. Haugsrud R, Norby T. High-temperature proton conductivity in acceptor-doped $LaNbO_4$. *Solid State Ionics*. 2006;177(13–14):1129–1135. https://doi.org/10.1016/j.ssi.2006.05.011

36. Besikiotis V, Knee CS, Ahmed I, Haugsrud R, Norby T. Crystal structure, hydration and ionic conductivity of the inherently oxygen-deficient $La_2Ce_2O_7$. *Solid State Ionics*. 2012;228:1–7. https://doi.org/10.1016/j.ssi.2012.08.023

37. Chesnaud A, Braida MD, Estradé S, *et al*. High-temperature anion and proton conduction in RE_3NbO_7 (RE=La, Gd, Y, Yb, Lu) compounds. *J Eur Ceram Soc*. 2015;35(11): 3051–3061. https://doi.org/10.1016/j.jeurceramsoc.2015.04.014

38. Mielewczyk-Gryn A, Navrotsky A. Enthalpies of formation of rare earth niobates, RE_3 NbO_7. *Am Mineral*. 2015;100(7):1578–1583. https://doi.org/10.2138/am-2015-5210

39. Mielewczyk-Gryn A, Wachowski S, Strychalska J, *et al*. Heat capacities and thermodynamic properties of antimony substituted lanthanum orthoniobates. *Ceram Int*. 2016;42(6):7054–7059. https://doi.org/10.1016/j.ceramint.2016.01.093

40. Mielewczyk-Gryn A, Navrotsky A. Enthalpies of formation of rare earth niobates, RE_3NbO_7. *Am Mineral*. 2015; 100: 1578–1583. https://doi.org/http://dx.doi.org/10.2138/am-2015-5210

41. Navrotsky A. Cation-distribution energetics and heats of mixing in $MgFe_2O_4$-$MgAl_2O_4$, $ZnFe_2O_4$-$ZnAl_2O_4$, and $NiAl_2O_4$-$ZnAl_2O_4$ spinels; study by high-temperature calorimetry. *Am Mineral*. 1986;71(9–10):1160–1169.

42. Shamblin J, Feygenson M, Neuefeind J, *et al.* Probing disorder in isometric pyrochlore and related complex oxides. *Nat Mater*. 2016; 15(5): 507–511. https://doi.org/10.1038/nmat4581

43. Drey D, O'Quinn EC, Gussev I, *et al.* Investigation of Disorder in $Ho_2Ti_{2-x}Zr_xO_7$: Pyrochlore to Defect Fluorite Chemical Series. *Prep*. 2019.

44. Boukamp B. A Nonlinear Least Squares Fit procedure for analysis of immittance data of electrochemical systems. *Solid State Ionics*. 1986; 20(1): 31–44. https://doi.org/10.1016/0167-2738(86)90031-7

45. Irvine JTS, Sinclair DC, West AR. Electroceramics: Characterization by Impedance Spectroscopy. *Adv Mater*. 1990;2(3):132–138. https://doi.org/10.1002/adma.19900020304

46. Wachowski S, Mielewczyk-Gryń A, Zagórski K, *et al*. Influence of Sb-substitution on ionic transport in lanthanum orthoniobates. *J Mater Chem A*. 2016;4(30):11696–11707. https://doi.org/10.1039/C6TA03403A

47. Norberg ST, Ahmed I, Hull S, Marrocchelli D, Madden P a. Local structure and ionic conductivity in the $Zr_2Y_2O_7$–Y_3NbO_7 system. *J Phys Condens Matter*. 2009;21(21):215401. https://doi.org/10.1088/0953-8984/21/21/215401

48. Boonlakhorn J, Thongbai P, Putasaeng B, Kidkhunthod P, Maensiri S, Chindaprasirt P. Microstructural evolution, non-Ohmic properties, and giant dielectric response in $CaCu_3Ti_{4-x}Ge_xO_{12}$ ceramics. *J Am Ceram Soc*. 2017;100(8):3478–3487. https://doi.org/10.1111/jace.14886

49. Fu Q, Tietz F, Stöver D. Electrical conductivity and redox behaviour of yttrium-substituted $SrTiO_3$: Dependence on preparation and processing procedures. *Proc - Electrochem Soc*. 2005;PV 2005-07:1417–1428. https://doi.org/10.1149/200507.1417pv

50. Lee J, Yashima M, Yoshimura M. Ionic conductivity of fluorite-structured solid solution $Y_{0.8}Nb_{0.2}O_{1.7}$. *Solid State Ionics*. 1998; 107: 47–51. http://dx.doi.org/10.1016/S0167-2738(97)00529-8

51. Uematsu K, Shinozaki K, Sakurai O, Mizutani N, Kato M. Electrical Conductivity of the System Y_2O_3 - TiO_2. *J Am Ceram Soc Notes*. 1979;62(3–4):219–221.

52. Yamaguchi S, Kobayashi K, Abe K, Yamazaki S, Iguchi Y. Electrical conductivity and thermoelectric power measurements of $Y_2Ti_2O_7$. *Solid State Ionics*. 1998. https://doi.org/10.1016/s0167-2738(98)00303-8

53. Kramer S, Spears M, Tuller HL. Conduction in titanate pyrochlores: role of dopants. *Solid State Ionics*. 1994. https://doi.org/10.1016/0167-2738(94)90125-2

54. Irvine JTS, Fagg DP, Labrincha J, Marques FMB. Development of novel anodes for solid oxide fuel cells. *Catal Today*. 1997; 38(4): 467–472. https://doi.org/10.1016/S0920-5861(97)00056-4

55. Kaiser A, Feighery AJ, Fagg DP, Irvine JTS. Electrical characterization of highly titania doped YSZ. *Ionics (Kiel)*. 1998;4(3–4):215–219. https://doi.org/10.1007/BF02375948

56. Irvine JTS, Feighery AJ, Fagg DP, García-Martín S. Structural studies on the optimization of fast oxide ion transport. *Solid State Ionics*. 2000;136–137:879–885. https://doi.org/10.1016/S0167-2738(00)00568-3

57. Kramer SA, Tuller HL. A novel titanate-based oxygen ion conductor: $Gd_2Ti_2O_7$. *Solid State Ionics*. 1995;82(1–2):15–23. https://doi.org/10.1016/0167-2738(95)00156-Z

58. Weppner W. Tetragonal zirconia polycrystals - a high performance solid oxygen ion conductor. *Solid State Ionics*. 1992; 52(1–3): 15–21. https://doi.org/10.1016/0167-2738(92)90087-6

59. Khan MS, Islam MS, Bates DR. Dopant substitution and ion migration in the $LaGaO_3$-based oxygen ion conductor. *J Phys Chem B*. 1998;102(17):3099–3104. https://doi.org/10.1021/jp972819d

60. Shimura T, Tanaka H, Matsumoto H, Yogo T. Influence of the transition-metal doping on conductivity of a $BaCeO_3$-based protonic conductor. *Solid State Ionics*. 2005; 176(39–40): 2945–2950. https://doi.org/10.1016/j.ssi.2005.09.027

61. Bohn H, Schober T. Electrical Conductivity of the High-Temperature Proton Conductor $BaZr_{0.9}Y_{0.1}O_{2.95}$. *J Am Ceram Soc*. 2000; 83(4): 768–772.

62. Navrotsky A. Thermodynamics of solid electrolytes and related oxide ceramics based on the fluorite structure. *J Mater Chem*. 2010; 20(47): 10577. https://doi.org/10.1039/c0jm01521k

63. Chen S, Costa GCC, Wang S, Munir ZA, Kim S, Navrotsky A. Grain-Boundary Enthalpies of Cubic Yttria-Stabilized Zirconia. *J Am Ceram Soc*. 2011; 94(7): 2181–2184. https://doi.org/10.1111/j.1551-2916.2010.04365.x

64. Aizenshtein M, Shvareva TY, Navrotsky A. Thermochemistry of Lanthana- and Yttria-Doped Thoria. *J Am Ceram Soc*. 2010; 93(12): 4142–4147. https://doi.org/10.1111/j.1551-2916.2010.04001.x

65. Avila-Paredes HJ, Shvareva T, Chen W, Navrotsky A, Kim S. A correlation between the ionic conductivities and the formation enthalpies of trivalent-doped ceria at relatively low temperatures. *Phys Chem Chem Phys*. 2009;11(38):8580. https://doi.org/10.1039/b821982f

66. Gonçalves MD, Maram PS, Muccillo R, Navrotsky A. Enthalpy of formation and thermodynamic insights into yttrium doped $BaZrO_3$. *J Mater Chem A*. 2014; 2(42): 17840–17847. https://doi.org/10.1039/C4TA03487B

67. Norberg ST, Hull S, Eriksson SG, Ahmed I, Kinyanjui F, Biendicho JJ. Pyrochlore to fluorite transition: The $Y_2(Ti_{1-x}Zr_x)_2O_7$ ($0.0 \geq x \geq 1.0$) System. *Chem Mater*. 2012;24(22):4294–4300. https://doi.org/10.1021/cm301649d

68. Norby T. Proton Conductivity in Perovskite Oxides. *Perovskite Oxide Solid Oxide Fuel Cells Fuel Cells Hydrog. Energy*. 2009:217–222.

69. Zohourian R, Merkle R, Raimondi G, Maier J. Mixed-conducting perovskites as cathode materials for protonic ceramic fuel cells: understanding the trends in proton uptake. *Adv Funct Mater*. 2018;1801241:1–10. https://doi.org/10.1002/adfm.201801241

70. Norby T, Widerøe M, Glöckner R, Larring Y. Hydrogen in oxides. *Dalt Trans*. 2004;(19):3012–3018.

71. Bjørheim TS, Hoedl MF, Merkle R, Kotomin EA, Maier J. Proton, Hydroxide Ion, and Oxide Ion Affinities of Closed-Shell Oxides: Importance for the Hydration Reaction and Correlation to Electronic Structure. *J Phys Chem C*. 2020;124:1277–1284. https://doi.org/10.1021/acs.jpcc.9b07570